

---

# Local Manifold Learning for No-Reference Image Quality Assessment

---

Timin Gao<sup>1</sup>, Wensheng Pan<sup>1</sup>, Yan Zhang<sup>1\*</sup>, Sicheng Zhao<sup>2</sup>, Shengchuan Zhang<sup>1</sup>  
Xiawu Zheng<sup>1</sup>, Ke Li<sup>3</sup>, Liujuan Cao<sup>1</sup>, Rongrong Ji<sup>1</sup>

<sup>1</sup>Key Laboratory of Multimedia Trusted Perception and Efficient Computing,  
Ministry of Education of China, Xiamen University  
<sup>2</sup>Harbin Institute of Technology <sup>3</sup>Tencent Youtu Lab  
timingao@stu.xmu.edu.cn

## Abstract

Contrastive learning has considerably advanced the field of Image Quality Assessment (IQA), emerging as a widely adopted technique. The core mechanism of contrastive learning involves minimizing the distance between quality-similar (positive) examples while maximizing the distance between quality-dissimilar (negative) examples. Despite its successes, current contrastive learning methods often neglect the importance of preserving the local manifold structure. This oversight can result in a high degree of similarity among hard examples within the feature space, thereby impeding effective differentiation and assessment. To address this issue, we propose an innovative framework that integrates local manifold learning with contrastive learning for No-Reference Image Quality Assessment (NR-IQA). Our method begins by sampling multiple crops from a given image, identifying the most visually salient crop. This crop is then used to cluster other crops from the same image as the positive class, while crops from different images are treated as negative classes to increase inter-class distance. Uniquely, our approach also considers non-saliency crops from the same image as intra-class negative classes to preserve their distinctiveness. Additionally, we employ a mutual learning framework, which further enhances the model's ability to adaptively learn and identify visual saliency regions. Our approach demonstrates a better performance compared to state-of-the-art methods in 7 standard datasets, achieving PLCC values of **0.942** (compared to 0.908 in TID2013) and **0.914** (compared to 0.894 in LIVEC).

## 1 Introduction

Image Quality Assessment (IQA) is a cornerstone of computer vision research, aiming to emulate the human visual system's subjective evaluation of image quality. Simply put, image quality assessment involves taking an input image and outputting a quality score based on its level of distortion. It finds application in numerous fields, including image restoration [1] and super-resolution images [2].

Although deep learning has greatly facilitated image quality assessment, there are still challenges. Commonly, some methods [3–7] employ or fine-tune classification models pre-trained on large datasets as feature extractors for predicting image quality scores. However, these models may not be ideally suited for IQA tasks. The complexity of IQA lies not only in discerning semantic information but also in contextual contrast and local sensitivity.

Thus, researchers have proposed self-supervised methods [8, 9] to tackle these challenges. They designate all crops extracted from the same image as positive classes while considering crops

---

\*Corresponding Author

from different images as negative classes. However, they overlook the variability in perceptual quality within different parts of the same image, leading to potential inaccuracies in quality assessment. Concretely, real-world scenarios reveal that image quality is intrinsically linked to content, influenced by diverse audience preferences [10, 11]. This complexity is reflected in the varying quality perceptions of different patches within the same image [12, 13], where local patch scores can differ from the overall image score. Additionally, when images are cropped multiple times to enhance training data, the local manifold of different crops from the same image tends to converge. This will cause the local manifold collapse and further affect the overall manifold structure as shown in Fig. 1. Specifically, when confronted with two images that share identical semantic content but exhibit varying degrees of distortion, the indistinguishability of their local manifolds may result in their distance (e.g.  $L1$  distance) in the feature space being very close. Such proximity can precipitate a collapse, resulting in imprecise quality score predictions. Hence, contrastive learning should encompass not only the differentiation of different images but also the finer distinction among different crops of the same image. In other words, maintaining intra-class distances to avoid local manifold collapse is essential to ensure accurate quality perception.

To address these challenges, we introduce a novel contrastive learning approach for NR-IQA rooted in Local Manifold Learning, named LML-IQA. It aims to refine the differentiation of feature manifolds not only between distinct samples but also within individual samples.

Specifically, we propose a mutual learning framework, incorporating both a teacher model and a student model. The teacher model is designed to sample visual saliency crops, which play a pivotal role in determining the corresponding overall image quality. Meanwhile, the student model is focused on the nuances of local manifold learning. In our approach, the teacher model crops the regions of the images with the highest attention weight. These visual saliency crops are considered positive classes. Other patches within the same image, as well as from different images, are used as negative classes.

This setup facilitates local manifold learning through contrastive mechanisms. The student model’s encoder compares these positive and negative classes using the InfoNCE loss, honing in on low-level quality perception details within images. Following this, the encoder output is fed into the student’s decoder, and the  $L1$  loss is computed between the decoder’s output and the ground truth, guiding the model to learn high-level quality scores. Besides, the student model undergoes continuous refinement, with the teacher model being updated regularly through the Exponential Moving Average (EMA) algorithm, ensuring the adaptive sampling of visual saliency crops to maintain the stability of local manifolds during the learning process. This innovative approach not only addresses the limitations of existing NR-IQA methods but also sets a new paradigm for accurately assessing image quality by considering both the intra-class and inter-class distances of features. Our contributions are the following:

- We introduce a novel contrastive learning approach, integrating a local manifold learning mechanism. To effectively maintain the integrity of the local manifold, we consider the visual non-saliency crops of an image as intra-class negative classes.
- Innovatively, we leverage the visual saliency crop of an image as the positive class. This inspiration is rooted in the recognition that the visual saliency crop is closely aligned with human visual observation characteristics and crucially determines the overall image quality.
- We employ a teacher-student mutual learning framework. It facilitates the adaptive extraction of visual saliency crops, crucial for preserving the stability of local manifolds during the learning process.

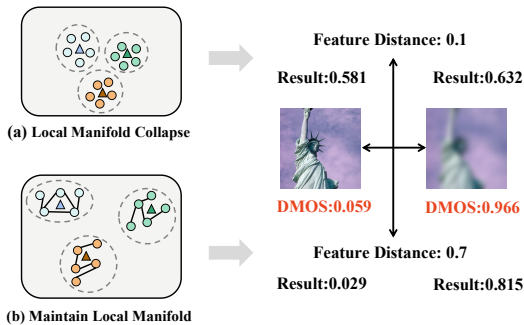


Figure 1: Comparison of the contrastive learning paradigm of IQA. (a) Previous contrastive learning-based IQA methods make crops of the same image converge, and fail to hold the local manifold; (b) Our approach preserves the local manifold and maintains the diversity of the feature space.

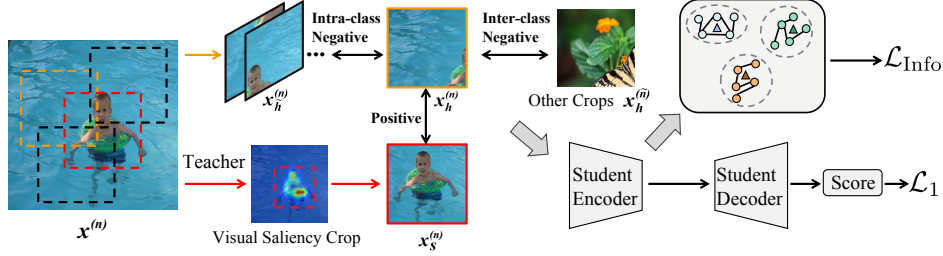


Figure 2: The overview of LML-IQA.

## 2 Related Work

The realm of Image Quality Assessment (IQA) encompasses diverse categories: Full-Reference (FR), Reduced-Reference (RR), and No-Reference (NR) methods, as evidenced by prior studies [14–19]. While procuring a reference image often poses challenges in real-world scenarios, NR-IQA methods offer a promising yet challenging alternative, directly estimating image quality independent of a reference image. This literature review delves into the ongoing research landscape concerning NR-IQA methods and local manifold learning.

### 2.1 NR-IQA based on Contrastive Learning

Recent years have witnessed the emergence of numerous self-supervised methods founded on the principles of contrastive learning within the realm of NR-IQA [9, 8, 20–22]. CONTRIQUE [9] pioneered an approach in which Madhusudana *et al.* categorized images sharing the same distortion type and degree into a class. This categorization facilitated the extraction of quality features through inter-class feature comparisons. It utilized distortion type and distortion level as class labels rather than employing the more specific and unique distortion quality of the image itself. This would limit the diversity of contrastive learning samples.

Subsequent research addressed this limitation. Saha *et al.* [8] treated each distinct distorted image as an independent class. Through extensive data augmentation and a specially crafted Intra-Pair Image Swapping Scheme, it generated comprehensive low-level representations of image quality, which were complementary to high-level features characterizing image content. Furthermore, Zhang *et al.* [22] extended their scope beyond image comparison by establishing a linkage between text and images using the CLIP model. It further improved the performance of NR-IQA by combining joint probability over multiple tasks.

These methods based on contrastive learning are dedicated to investigating distinct pretext tasks and employing diverse data augmentation strategies to bolster quality perception. They posit that distinct crops of the same image share equivalent quality perception. Consequently, their positive classes are derived from assorted random crops of the same image. However, they ignore the differences within the sample, which can lead to local manifold collapse. Considering the human visual perception system, an image’s perceptual quality is primarily influenced by its prominent regions. Our method addresses these concerns by introducing intra-class negative classes and visual saliency cropping.

### 2.2 Manifold Learning in Image Quality Assessment

In the realm of computer vision, Local Manifold Learning [23, 24] (LML) stands as an unsupervised algorithmic approach, aiming to elucidate the intrinsic low-dimensional manifold structures embedded within high-dimensional data spaces. Jiang *et al.* [25] ingeniously applied manifold learning to reduce the dimensionality of RGB images, and effectively predicted the quality of stereoscopic images by constructing a low-dimensional representation that mimics human visual perception. Guan *et al.* [26] presented an innovative no-reference quality assessment method for High-Dynamic-Range (HDR) images, where manifold learning is adeptly employed on the first feature map to discern the intrinsic geometric structure of high-dimensional data in a low-dimensional space, enhancing the accuracy of HDR image quality prediction. These methods primarily utilize traditional data dimensionality reduction techniques, excluding the application of deep learning strategies. We leverage contrastive

learning to extract data manifold, harnessing deep learning algorithms to reveal complex underlying structures within the data manifold.

### 3 Method

#### 3.1 Overview

In this paper, we propose an NR-IQA model named LML-IQA based on contrastive learning, and its specific framework is shown in Fig. 2. We divide the model into a teacher and a student model. The teacher model is responsible for the visual saliency cropping of images, using the cropped images as positive classes for the student’s contrastive learning. Positive classes with visual saliency can increase the consistency and representativeness of contrastive learning. The student model is responsible for two subtasks, including contrastive learning and image quality prediction, which share a feature extractor for joint optimization. By comparing the saliency image with other non-saliency images, the model’s attention to local important areas of the image has been strengthened, simulating human attention to saliency regions in image quality perception. Additionally, to enhance the precision of the teacher’s visual saliency cropping and provide more consistent positive instances for contrastive learning, we employ the EMA algorithm to update the teacher model.

#### 3.2 Local Manifold Learning

The classic quality-aware pretext task treats each image instance with different quality as different classes. Specifically, the crops from the same image are positive, while the crops from different images are negative. These methods prioritize inter-class distance, disregarding intra-class distance, which leads to potential local manifold collapse. We present a novel contrastive learning method based on local manifold learning. Introducing the visual saliency cropping, we consider the saliency regions within the input image as positive class. To maintain local manifold integrity, we define the crops of non-significant regions as intra-class negative classes. Simultaneously, all other images are cropped to serve as inter-class negative classes, enhancing the differentiation of the overall manifold structure. The negative classes combined with the positive class make the crops close enough to maintain a consistent representation, but not very close to letting the local manifold collapse.

##### 3.2.1 Visual Saliency Cropping

We believe that treating different random cropping of the same degraded image as positive classes lacks representativeness to some extent. It provides limited quality perception guidance for contrastive learning. Because in the human perception system, humans tend to pay more attention to the salient regions in the image, which also means that the image quality score largely depends on the salient regions of the image. Therefore, we introduce visual saliency cropping. We obtain positive classes corresponding to the image by cropping the visual saliency of the image. We feed the image into the teacher model, select the salient regions of the current image through the self-attention mechanism of the teacher model, and crop them.

Specifically, we reshape the image  $224 \times 224$ , divide it into  $T$  patches, and add an additional learnable class token to feed into Vision Transformer. Three linear projection layers are employed to convert  $T + 1$  tokens into matrices  $\mathbf{Q}, \mathbf{K}, \mathbf{V} \in \mathbb{R}^{(T+1) \times D}$ , representing the query, key, and value, respectively. Through the self-attention operation, we obtain an attention map  $\mathbf{A}_{t2t} \in \mathbb{R}^{(T+1) \times (T+1)}$  and  $\mathbf{A}_{t2t} = \text{softmax}(\mathbf{Q}\mathbf{K}^\top / \sqrt{D})$  that represents the degree of attention each token has on other tokens. From the global pairwise attention map  $\mathbf{A}_{t2t}$ , we can extract the class-to-patch attention  $\mathbf{A}_{c2p}$ , where  $\mathbf{A}_{c2p} = \mathbf{A}_{t2t}[0, 1 : T + 1]$ . Considering that higher layers learn more advanced discriminative representations, while lower layers capture more general and low-level visual information. We propose to fuse the token to token attention from the last  $K$  transformer encoding layers to ensure the accuracy of image saliency judgment. Then we set the  $\hat{\mathbf{A}}_{c2p}$  shape as  $\mathbb{R}^{\sqrt{T} \times \sqrt{T}}$ , and select the area on it with the highest attention of  $M \times M$ . In other words, we select the  $M \times M$  area with the highest sum of attention weights as the saliency region of this image. The process is as follows:

$$\hat{\mathbf{A}}_{c2p} = \frac{1}{K} \sum_l^{l+K} \mathbf{A}_{c2p}^l, \tag{1}$$

Table 1: Definition of positive pair, intra-class negative pair, and inter-class negative pair in the pretext task.

Positive Pair	Intra-class negative pair	Inter-class negative pair
$(\mathbf{x}_h^{(n)}, \mathbf{x}_s^{(n)})$	$(\mathbf{x}_h^{(n)}, \mathbf{x}_h^{(n)})$	$(\mathbf{x}_h^{(n)}, \mathbf{x}_s^{(\tilde{n})})$

$$\arg \max_{p,q} = \sum_{i=0}^M \sum_{j=0}^M \hat{\mathbf{A}}_{c2p}[p+i, q+j]. \quad (2)$$

We use this region as a positive class for the input image in subsequent contrastive learning.

### 3.2.2 Quality-Aware Training

In the context of contrastive learning for image quality assessment, the typical approach involves randomly cropping two patches from the same distorted image, where this pair makes up a positive class and the negative class is cropped from another distorted image. However, we contend that utilizing two randomly cropped patches from the same image as a positive pair may not be the optimal choice. The perceived quality of different positions within the same image can vary significantly, and humans allocate varying levels of attention to the image’s center regions and edge. The saliency regions in the original image are more representative of the perceived quality of the entire image. So our expectation is that pairing positive classes will align the quality features of the cropped image more closely with the quality attributes of the visually salient regions in the original image. Specifically, let us consider  $N$  distorted images denoted as  $x^1, x^2 \dots x^N$ . From each image, we extract positive and negative samples to facilitate the contrastive learning process. The extracted samples include randomly cropping each image  $x^n$   $H$  times to generate different “views” denoted as  $x_1^n, x_2^n \dots x_H^n$ , and the salient region of the image  $x^n$ , denoted by  $x_s^n$ . Within a single batch, the patch  $x_i^n$  and its corresponding salient region  $x_s^n$  form a positive pair. The patch  $x_i^n$  and all non-salient regions form negative pairs, including both intra-class negative pairs and inter-class negative pairs, as shown in Table 1.

The input patch  $\mathbf{x}^n$  undergoes processing through Transformer’s encoder  $\mathcal{F}$  to derive the final feature  $\mathbf{f}_h^{(n)} = \mathcal{F}(\mathbf{x}_h^{(n)}) / \|\mathcal{F}(\mathbf{x}_h^{(n)})\|$  for contrastive learning. The InfoNCE loss function is utilized to calculate the quality comparison loss between “query” and “key” patches within each batch. For a given image  $x^n$ , it is defined as follows:

$$\mathcal{P}_{\text{Intra}}^n = \sum_{\tilde{h} \neq h}^H \exp(\mathbf{f}_h^{(n)} \cdot \mathbf{f}_{\tilde{h}}^{(n)} / \tau), \quad (3)$$

$$\mathcal{P}_{\text{Inter}}^n = \sum_{\tilde{n} \neq n}^N \sum_{h'=1}^H \exp(\mathbf{f}_h^{(n)} \cdot \mathbf{f}_{h'}^{(\tilde{n})} / \tau), \quad (4)$$

$$\mathcal{L}_{\text{Info}}^n = -\log \frac{\exp(\mathbf{f}_h^{(n)} \cdot \mathbf{f}_s^{(n)} / \tau)}{\mathcal{P}_{\text{Intra}}^n + \mathcal{P}_{\text{Inter}}^n}, \quad (5)$$

where  $\mathcal{P}_{\text{Intra}}^n$  and  $\mathcal{P}_{\text{Inter}}^n$  represent calculations within and between classes, respectively,  $\tau$  is a temperature hyper-parameter,  $N$  is the number of images present in the batch, and  $H$  represents the number of times the image is cropped. In the **Appendix A**, a qualitative analysis of Eq. 5 is provided, confirming the superiority of our proposed method over traditional contrastive learning.

Furthermore, we process the output of Transformer Decoder  $\mathcal{G}$  to determine the quality score  $\hat{Y}_h^n = \text{MLP}(\mathcal{G}(\mathcal{F}(x_h^n)))$  associated with each patch  $x_h^n$ .

Subsequently, we compute the  $\mathcal{L}1$  loss between the predicted score  $\hat{Y}_h^n$  and the ground truth  $Y_h^n$ :

$$\mathcal{L}_1^n = \sum_{h=1}^H \|\hat{Y}_h^n - Y_h^n\|_1. \quad (6)$$

Table 2: Performance comparison measured by averages of SRCC and PLCC on standard IQA datasets, where bold entries indicate the best results, underlines indicate the second-best.

Method	LIVE		CSIQ		TID2013		KADID		LIVEC		KonIQ		LIVEFB		SPAQ	
	PLCC	SRCC	PLCC	SRCC	PLCC	SRCC	PLCC	SRCC	PLCC	SRCC	PLCC	SRCC	PLCC	SRCC	PLCC	SRCC
DIIVINE [15]	0.908	0.892	0.776	0.804	0.567	0.643	0.435	0.413	0.591	0.588	0.558	0.546	0.187	0.092	0.600	0.599
BRISQUE [27]	0.944	0.929	0.748	0.812	0.571	0.626	0.567	0.528	0.629	0.629	0.685	0.681	0.341	0.303	0.817	0.809
ILNIQE [28]	0.906	0.902	0.865	0.822	0.648	0.521	0.558	0.534	0.508	0.508	0.537	0.523	0.332	0.294	0.712	0.713
BIECON [29]	0.961	0.958	0.823	0.815	0.762	0.717	0.648	0.623	0.613	0.613	0.654	0.651	0.428	0.407	-	-
MEON [30]	0.955	0.951	0.864	0.852	0.824	0.808	0.691	0.604	0.710	0.697	0.628	0.611	0.394	0.365	-	-
WaDIQaM [31]	0.955	0.960	0.844	0.852	0.855	0.835	0.752	0.739	0.671	0.682	0.807	0.804	0.467	0.455	-	-
DBCNN [13]	0.971	0.968	0.959	0.946	0.865	0.816	0.856	0.851	0.869	0.851	0.884	0.875	0.551	0.545	0.915	0.911
MetalQA [32]	0.959	0.960	0.908	0.899	0.868	0.856	0.775	0.762	0.835	0.802	0.887	0.850	0.540	0.507	-	-
P2P-BM [12]	0.958	0.959	0.902	0.899	0.856	0.862	0.849	0.84	0.842	0.844	0.885	0.872	0.598	0.526	-	-
HyperIQA [7]	0.966	0.962	0.942	0.923	0.858	0.840	0.845	0.852	0.882	0.859	0.917	0.906	0.602	0.544	0.915	0.911
TIQA [33]	0.965	0.949	0.838	0.825	0.858	0.846	0.855	0.85	0.861	0.845	0.903	0.892	0.581	0.541	-	-
MUSIQ [3]	0.911	0.940	0.893	0.871	0.815	0.773	0.872	0.875	0.746	0.702	0.928	0.916	0.661	0.566	0.921	0.918
TReS [4]	0.968	0.969	0.942	0.922	0.883	0.863	0.858	0.859	0.877	0.846	0.928	0.915	0.625	0.554	-	-
DACNN [34]	0.980	0.978	0.957	0.943	0.889	0.871	0.905	0.905	0.884	0.866	0.912	0.901	-	-	0.921	0.915
CONTRIQUE [9]	0.961	0.960	0.955	0.942	0.857	0.843	<b>0.937</b>	<b>0.934</b>	0.857	0.845	0.906	0.894	0.641	<u>0.580</u>	0.919	0.914
Re-IQA [8]	0.971	0.970	0.960	<u>0.947</u>	0.861	0.804	0.885	0.872	0.854	0.840	0.923	0.914	-	-	<u>0.925</u>	0.918
DEIQT [5]	0.982	0.980	0.963	0.946	0.908	0.892	0.887	0.889	0.894	0.875	0.934	0.921	0.663	0.571	0.923	0.919
LML-IQA (Ours)	<b>0.984</b>	<b>0.982</b>	<b>0.977</b>	<b>0.968</b>	<b>0.942</b>	<b>0.931</b>	<u>0.918</u>	<u>0.915</u>	<b>0.914</b>	<b>0.891</b>	<b>0.938</b>	<b>0.923</b>	<b>0.673</b>	<b>0.585</b>	<b>0.926</b>	<b>0.921</b>
std	±0.003	±0.003	±0.003	±0.005	±0.011	±0.014	±0.005	±0.005	±0.006	±0.013	±0.001	±0.0002	±0.011	±0.001	±0.001	±0.002

### 3.2.3 Final Loss for IQA Learning

The total loss includes a contrastive loss and a  $L1$  loss for ground truth. The contrastive loss is employed to capture distinctions among various distortions, while the  $L1$  loss additionally steers the prediction of quality scores. The ultimate loss is computed as follows:

$$\mathcal{L} = \sum_{n=1}^N ((1 - \alpha)\mathcal{L}_1^n + \alpha\mathcal{L}_{\text{Info}}^n), \quad (7)$$

where  $\alpha$  is the balance factor between two losses, and  $N$  is the number of images present in the batch.

### 3.3 Teacher-Student Mutual Learning

We develop a mutual learning framework involving a teacher and a student. In particular, we employ a teacher model for the visual saliency cropping. The student model utilizes visual saliency crops as positive classes for contrastive learning and then updates the teacher model. To enhance the precision of quality perception for the teacher (spanning from the initial stage focused on pure significance objectives to subsequent significant areas influencing quality), and to offer more consistent positive instances for contrastive learning, we employ the EMA algorithm to update the teacher model. Specifically, the weights of the teacher model can be expressed as follows:

$$\theta_t \leftarrow \beta\theta_t + (1 - \beta)\theta_s, \quad (8)$$

where  $\theta_t$  is the teacher model weight,  $\theta_s$  is the student model weight, and  $\beta$  is the EMA coefficient. The mutual learning paradigm enhances the precision and stability of visual saliency cropping within the teacher model, simultaneously providing improved guidance for the student model.

## 4 Experiments

### 4.1 Benchmark Datasets and Evaluation Protocols

The effectiveness of the LML-IQA model is assessed using eight standard NR-IQA datasets. This set comprises four synthetic datasets: LIVE [35], CSIQ [36], TID2013 [37], and KADID [38], along with four authentic datasets: LIVEC [39], KonIQ [40], LIVEFB [12], and SPAQ [41]. The synthetic dataset is generated by applying various types of distortions, such as Gaussian blur and random noise, to a restricted set of original images. Conversely, the authentic dataset is captured by different photographers using a variety of mobile devices, thereby capturing more genuine distortions that occur in natural environments.

Table 3: SRCC on the cross datasets validation, where bold entries and underlines indicate the best results and the second-best.

Training	LIVEFB	LIVEC	KonIQ	LIVE	CSIQ
Testing	LIVEC	KonIQ	LIVEC	CSIQ	LIVE
DBCNN [13]	0.724	0.754	0.755	0.758	0.877
P2P-BM [12]	0.738	0.740	0.770	0.712	-
HyperIQA [7]	0.735	<b>0.772</b>	0.785	0.744	0.926
TReS [4]	0.740	0.733	0.786	0.761	-
DEIQT[5]	<b>0.781</b>	0.744	<u>0.794</u>	<u>0.781</u>	<u>0.932</u>
LML-IQA(Ours)	<u>0.763</u>	<u>0.756</u>	<b>0.818</b>	<b>0.833</b>	<b>0.951</b>

For the evaluation of the LML-IQA model’s predictive accuracy and monotonicity, we employ two widely accepted standard evaluation metrics: Spearman Rank Correlation Coefficient (SRCC) and Pearson Linear Correlation Coefficient (PLCC). These evaluation metrics are universally recognized, yielding values within the range of 0 to 1, with higher values indicating greater predictive capability.

## 4.2 Implementation Details

For the training of LML-IQA, we follow a standard procedure, randomly cropping the input image into ten patches along with one patch containing a saliency region, each with a resolution of  $224 \times 224$  pixels. For the model architecture, we adopt the ViT-S Transformer encoder proposed in DeiT III [42]. The attention score is calculated as the average of the last three layers of the encoder. As for the decoder, we utilize a Transformer Decoder with a depth of 1. The model undergoes 9 training epochs, utilizing a learning rate of  $2 \times 10^{-4}$ . Moreover, a decay factor of 10 is applied every 3 epochs. The parameter  $\beta$  in Eq. 8 is set to 0.999. The batch size is adjusted based on the dataset size. To ensure a comprehensive evaluation, we partition the dataset randomly into an 80% training set and a 20% testing set. To mitigate performance bias, we repeat this process ten times and report the average values of PLCC and SRCC. All the experiments are carried out on 4 NVIDIA 3090 GPUs.

## 4.3 Overall Prediction Performance Comparison

Table 2 presents the performance of LML-IQA across eight datasets, with synthetic datasets on the left and authentic datasets on the right. Our approach achieves either the best or second-best performance on all datasets. Notably, LML-IQA demonstrates significant improvements in the CSIQ and TID2023. In terms of SRCC, LML-IQA shows enhancements of 0.022 and 0.039 compared to the second-best method, respectively. This improvement is attributed to the introduction of visual saliency cropping and intra-class negative classes, which enhance the model’s sensitivity to image quality variations and prevent the degradation of the manifold structure. Given the diversity of image content and the wide range of distortion types, achieving competitive performance on these datasets is a challenging task. Therefore, these observations confirm the effectiveness of LML-IQA in accurately characterizing image quality.

## 4.4 Generalization Capability Validation

To further assess the generalization ability of LML-IQA, we conduct cross-dataset validation experiments. Specifically, our model is trained on one dataset and subsequently tested on another dataset without any fine-tuning or parameter adaptation. To ensure simplicity and universality, we conduct several experiments. The experimental outcomes, represented by the average SRCC values across these datasets, are presented in Table 3. Notably, in five of the experiments, LML-IQA has demonstrated the highest or second-highest performance. Furthermore, certain cross-dataset performances have exceeded those of previous supervised methods in Table 2. By incorporating contrastive learning into the model, we ensure that the model goes beyond merely fitting to the labels of the training dataset, capturing crucial image quality features more effectively. Through intra-class and inter-class comparisons, the model preserves the local manifold and simultaneously achieves a manifold structure with robust generalization capabilities.

Table 4: Ablation experiments on LIVEC and TID datasets. Bold indicates best performance.

Module	LIVEC		TID	
	PLCC	SRCC	PLCC	SRCC
Baseline	0.887	0.870	0.896	0.873
std	$\pm 0.007$	$\pm 0.015$	$\pm 0.050$	$\pm 0.063$
+ Random Crop	0.894	0.874	0.904	0.885
std	$\pm 0.006$	$\pm 0.008$	$\pm 0.069$	$\pm 0.082$
+ Visual Saliency Crop	0.903	0.883	0.918	0.902
std	$\pm 0.011$	$\pm 0.012$	$\pm 0.022$	$\pm 0.027$
+ Mutual Learning	0.910	0.884	0.934	0.920
std	$\pm 0.007$	$\pm 0.017$	$\pm 0.011$	$\pm 0.015$
LML-IQA	<b>0.914</b>	<b>0.891</b>	<b>0.942</b>	<b>0.931</b>
std	$\pm 0.007$	$\pm 0.013$	$\pm 0.011$	$\pm 0.014$

Table 5: Analysis of the M in Visual Saliency Cropping on both synthetic and authentic datasets.

$M \times M$	CSIQ		LIVEC	
	PLCC	SRCC	PLCC	SRCC
$5 \times 5$	0.975	0.966	0.910	0.885
$6 \times 6$	0.974	0.965	0.906	0.885
$7 \times 7$	0.974	0.965	0.906	0.884
$8 \times 8$	<b>0.977</b>	<b>0.968</b>	<b>0.914</b>	<b>0.891</b>
$9 \times 9$	0.974	0.965	0.907	0.885
$10 \times 10$	0.973	0.963	0.905	0.880

#### 4.5 Ablation Study

LML-IQA is an innovative method based on local manifold learning, consisting of two essential components: visual saliency cropping and teacher-student mutual learning. As shown in Table 4, we further investigate the impact of each component on the overall performance of the model.

**Effective on Random Crop and Visual Saliency Crop.** We attempt contrastive learning based on random cropping (i.e., take two crops from the same image as positive classes and crops from different images as negative classes). It can be seen that contrastive learning indeed helps the model learn more essential image quality expressions. Subsequently, we introduce visual saliency cropping to compare the random cropping. It further improves the performance of the model. This phenomenon further supports our motivation: the perception of image quality comes more from the saliency region of the image. Aligning the crop with the saliency region of the image helps to strengthen the correlation between positive classes in contrastive learning and provides more accurate guidance for contrastive learning. It is worth noting that we use the teacher to perform visual saliency cropping on the images before the training process begins, and obtain fixed visual saliency regions as positive classes.

**Effective on Mutual Learning and EMA.** To dynamically adjust the visual saliency regions of the image, we introduce a model of teacher-student mutual learning. Before each training epoch, we use the teacher to perform visual saliency cropping on the images, and after each training epoch, we use the student to update the teacher. Compared to freezing the teacher (fixing visual saliency cropping), the update of the teacher model enables real-time updates of the salient area of the image during each epoch, which helps the teacher model provide more accurate visual saliency cropping. The guidance of student models helps teacher shift their focus from the initial salient objects to areas that truly significantly affect the overall image quality perception. Besides, to prevent the weight update of the teacher model from being too fast, which results in a significant difference in visual saliency cropping on the same image between adjacent epochs, hindering contrastive learning. We use the EMA algorithm to update the teacher model. Delaying the update of the teacher model helps to compare sample features that are more consistent before and after learning, while also making the model more focused on the saliency area of the image.

In summary, the ablation experiment demonstrates the significant contribution of each component to the overall performance of LML-IQA. The proposed visual saliency cropping and teacher-student mutual learning provide significant improvements in model accuracy and stability, and their combination promotes advanced deep-learning models for image quality assessment.

#### 4.6 Analysis of the M in Visual Saliency Cropping

We study the influence of the visual saliency cropping size, denoted as  $M \times M$ . Our experiment encompasses both synthetic dataset CSIQ and authentic dataset LIVEC, respectively, where we explore a range of  $M$ -values spanning from 5 to 10. The results, as presented in Table 5, consistently indicate that the performance remains stable across different  $M$  values, exhibiting only fluctuations of less than 1%. As the cropping patch size increases, the model acquires additional reference



Table 6: Data-efficient learning validation with the training set containing 20%, 40% and 60% images. Bold entries indicate the best performance.

Training Set	Methods	LIVE		LIVEC		KonIQ	
		PLCC	SRCC	PLCC	SRCC	PLCC	SRCC
20%	ViT-BIQA	0.828	0.894	0.641	0.622	0.855	0.825
	HyperNet	0.950	0.951	0.809	0.776	0.873	0.869
	DEIQT	0.968	0.965	0.822	0.792	0.908	0.888
	LML-IQA	<b>0.976</b>	<b>0.974</b>	<b>0.841</b>	<b>0.811</b>	<b>0.917</b>	<b>0.898</b>
40%	ViT-BIQA	0.847	0.903	0.714	0.684	0.901	0.880
	HyperNet	0.961	0.959	0.849	0.832	0.908	0.892
	DEIQT	0.973	0.971	0.855	0.838	0.922	0.903
	LML-IQA	<b>0.979</b>	<b>0.977</b>	<b>0.878</b>	<b>0.852</b>	<b>0.929</b>	<b>0.911</b>
60%	ViT-BIQA	0.856	0.915	0.739	0.705	0.916	0.903
	HyperNet	0.963	0.960	0.862	0.843	0.914	0.901
	DEIQT	0.974	0.972	0.877	0.848	0.931	0.914
	LML-IQA	<b>0.981</b>	<b>0.979</b>	<b>0.898</b>	<b>0.877</b>	<b>0.931</b>	<b>0.915</b>

information concerning visual saliency regions, thus aiding in improved contrastive learning. When the cropped size is  $8 \times 8$ , the model achieves optimal performance on both the CSIQ and LIVEC datasets. However, with the further expansion of the visual saliency area, the saliency features tend to diminish, introducing non-visual saliency cues that potentially have a detrimental impact on the model’s efficacy and performance.

#### 4.7 Data-Efficient Learning Validation

Considering the expensive costs of image annotation and model training, data-efficient learning is a crucial issue in IQA. LML-IQA, through local manifold learning, enables the model to adequately capture perceptual differences in image quality with limited data, significantly reducing the training data requirement.

To comprehensively explore this characteristic, we conduct a controlled experiment, progressively varying the training data volume in 20% increments from 20% to 60%. This process is repeated ten times for each training data volume, with the average of the performance being reported. The test dataset consistently comprises 20% of the images and does not overlap with the training data in all trials. Detailed experimental results are presented in Table 6. Our method consistently outperforms other state-of-the-art NR-IQA methods using comparable training data volumes. Remarkably, LML-IQA attains competitive performance with other methods on the LIVE and CSIQ datasets (Table 2) using just 40% of the training data. With the training data volume reaching 60%, LML-IQA surpasses all other methods. In summary, by employing saliency cropping to obtain regions most closely correlated with image quality, and conducting local manifold learning on these areas, our method excels in extracting image-quality information, facilitating data-efficient learning.

## 5 Conclusion

This paper introduces LML-IQA, an innovative No-Reference Image Quality Assessment (NR-IQA) model grounded in local manifold learning. Central to this approach is the strategic use of visual saliency cropping and intra-class negative classes. This ensures a consistent representation, while simultaneously avoiding excessive proximity to prevent local manifold collapse. In parallel, inter-class negative classes are utilized to partition the overall manifold structure, ensuring a robust and comprehensive image quality assessment. Furthermore, we establish a mutual learning paradigm between the teacher and student through the EMA algorithm. This approach facilitates adaptive adjustments in visual saliency cropping, maintaining the stability of local manifolds during the learning process. Experimental results conducted on eight IQA datasets highlight the superiority of our proposed approach.

## References

- [1] Mark R Banham and Aggelos K Katsaggelos. Digital image restoration. *IEEE signal processing magazine*, 14(2):24–41, 1997.
- [2] Chao Dong, Chen Change Loy, Kaiming He, and Xiaoou Tang. Image super-resolution using deep convolutional networks. *IEEE transactions on pattern analysis and machine intelligence*, 38(2):295–307, 2015.
- [3] Junjie Ke, Qifei Wang, Yilin Wang, Peyman Milanfar, and Feng Yang. Musiq: Multi-scale image quality transformer. In *Proceedings of the IEEE/CVF International Conference on Computer Vision*, pages 5148–5157, 2021.
- [4] S Alireza Golestaneh, Saba Dadsetan, and Kris M Kitani. No-reference image quality assessment via transformers, relative ranking, and self-consistency. In *Proceedings of the IEEE/CVF Winter Conference on Applications of Computer Vision*, pages 1220–1230, 2022.
- [5] Guanyi Qin, Runze Hu, Yutao Liu, Xiawu Zheng, Haotian Liu, Xiu Li, and Yan Zhang. Data-efficient image quality assessment with attention-panel decoder. In *Proceedings of the Thirty-Seventh AAAI Conference on Artificial Intelligence*, 2023.
- [6] Hossein Talebi and Peyman Milanfar. Nima: Neural image assessment. *IEEE transactions on image processing*, 27(8):3998–4011, 2018.
- [7] Shaolin Su, Qingsen Yan, Yu Zhu, Cheng Zhang, Xin Ge, Jinqiu Sun, and Yanning Zhang. Blindly assess image quality in the wild guided by a self-adaptive hyper network. In *Proceedings of the IEEE/CVF Conference on Computer Vision and Pattern Recognition*, pages 3667–3676, 2020.
- [8] Avinab Saha, Sandeep Mishra, and Alan C Bovik. Re-iqa: Unsupervised learning for image quality assessment in the wild. In *Proceedings of the IEEE/CVF Conference on Computer Vision and Pattern Recognition*, pages 5846–5855, 2023.
- [9] Pavan C Madhusudana, Neil Birkbeck, Yilin Wang, Balu Adsumilli, and Alan C Bovik. Image quality assessment using contrastive learning. *IEEE Transactions on Image Processing*, 31:4149–4161, 2022.
- [10] Dingquan Li, Tingting Jiang, Weisi Lin, and Ming Jiang. Which has better visual quality: The clear blue sky or a blurry animal? *IEEE Transactions on Multimedia*, 21(5):1221–1234, 2018.
- [11] Wei Sun, Xiongkuo Min, Danyang Tu, Siwei Ma, and Guangtao Zhai. Blind quality assessment for in-the-wild images via hierarchical feature fusion and iterative mixed database training. *IEEE Journal of Selected Topics in Signal Processing*, 2023.
- [12] Zhenqiang Ying, Haoran Niu, Praful Gupta, Dhruv Mahajan, Deepti Ghadiyaram, and Alan Bovik. From patches to pictures (paq-2-piq): Mapping the perceptual space of picture quality. In *Proceedings of the IEEE/CVF Conference on Computer Vision and Pattern Recognition*, pages 3575–3585, 2020.
- [13] Weixia Zhang, Kede Ma, Jia Yan, Dexiang Deng, and Zhou Wang. Blind image quality assessment using a deep bilinear convolutional neural network. *IEEE Transactions on Circuits and Systems for Video Technology*, 30(1):36–47, 2018.
- [14] Xinhao Liu, Masayuki Tanaka, and Masatoshi Okutomi. Single-image noise level estimation for blind denoising. *IEEE Trans. Image Process.*, 22(12):5226–5237, 2013.
- [15] Michele A Saad, Alan C Bovik, and Christophe Charrier. Blind image quality assessment: A natural scene statistics approach in the dct domain. *IEEE transactions on Image Processing*, 21(8):3339–3352, 2012.
- [16] Guangtao Zhai, Xiaolin Wu, Xiaokang Yang, Weisi Lin, and Wenjun Zhang. A psychovisual quality metric in free-energy principle. *IEEE Trans. Image Process.*, 21(1):41–52, 2011.
- [17] Ke Gu, Guangtao Zhai, Xiaokang Yang, and Wenjun Zhang. Using free energy principle for blind image quality assessment. *IEEE Transactions on Multimedia*, 17(1):50–63, 2014.

- [18] Zhou Wang, Hamid R Sheikh, and Alan C Bovik. No-reference perceptual quality assessment of jpeg compressed images. In *Proceedings. International conference on image processing*, volume 1, pages I–I. IEEE, 2002.
- [19] Anush Krishna Moorthy and Alan Conrad Bovik. Blind image quality assessment: From natural scene statistics to perceptual quality. *IEEE Trans. Image Process.*, 20(12):3350–3364, 2011.
- [20] Kai Zhao, Kun Yuan, Ming Sun, Mading Li, and Xing Wen. Quality-aware pre-trained models for blind image quality assessment. In *Proceedings of the IEEE/CVF Conference on Computer Vision and Pattern Recognition*, pages 22302–22313, 2023.
- [21] Ashish Jaiswal, Ashwin Ramesh Babu, Mohammad Zaki Zadeh, Debapriya Banerjee, and Fillia Makedon. A survey on contrastive self-supervised learning. *Technologies*, 9(1):2, 2020.
- [22] Weixia Zhang, Guangtao Zhai, Ying Wei, Xiaokang Yang, and Kede Ma. Blind image quality assessment via vision-language correspondence: A multitask learning perspective. In *Proceedings of the IEEE/CVF Conference on Computer Vision and Pattern Recognition*, pages 14071–14081, 2023.
- [23] Li Ma, Melba M Crawford, and Jinwen Tian. Local manifold learning-based  $k$ -nearest-neighbor for hyperspectral image classification. *IEEE Transactions on Geoscience and Remote Sensing*, 48(11):4099–4109, 2010.
- [24] Charles K Chui and Hrushikesh N Mhaskar. Deep nets for local manifold learning. *Frontiers in Applied Mathematics and Statistics*, 4:12, 2018.
- [25] Gangyi Jiang, Meiling He, Mei Yu, Feng Shao, and Zongju Peng. Perceptual stereoscopic image quality assessment method with tensor decomposition and manifold learning. *IET Image Processing*, 12(5):810–818, 2018.
- [26] Feifan Guan, Gangyi Jiang, Yang Song, Mei Yu, Zongju Peng, and Fen Chen. No-reference high-dynamic-range image quality assessment based on tensor decomposition and manifold learning. *Applied Optics*, 57(4):839–848, 2018.
- [27] Anish Mittal, Anush Krishna Moorthy, and Alan Conrad Bovik. No-reference image quality assessment in the spatial domain. *IEEE Transactions on image processing*, 21(12):4695–4708, 2012.
- [28] Lin Zhang, Lei Zhang, and Alan C Bovik. A feature-enriched completely blind image quality evaluator. *IEEE Transactions on Image Processing*, 24(8):2579–2591, 2015.
- [29] Jongyoo Kim and Sanghoon Lee. Fully deep blind image quality predictor. *IEEE Journal of selected topics in signal processing*, 11(1):206–220, 2016.
- [30] Kede Ma, Wentao Liu, Kai Zhang, Zhengfang Duanmu, Zhou Wang, and Wangmeng Zuo. End-to-end blind image quality assessment using deep neural networks. *IEEE Transactions on Image Processing*, 27(3):1202–1213, 2017.
- [31] Sebastian Bosse, Dominique Maniry, Klaus-Robert Müller, Thomas Wiegand, and Wojciech Samek. Deep neural networks for no-reference and full-reference image quality assessment. *IEEE Transactions on image processing*, 27(1):206–219, 2017.
- [32] Hancheng Zhu, Leida Li, Jinjian Wu, Weisheng Dong, and Guangming Shi. MetaIqa: Deep meta-learning for no-reference image quality assessment. In *Proceedings of the IEEE/CVF Conference on Computer Vision and Pattern Recognition*, pages 14143–14152, 2020.
- [33] Junyong You and Jari Korhonen. Transformer for image quality assessment. In *2021 IEEE International Conference on Image Processing (ICIP)*, pages 1389–1393. IEEE, 2021.
- [34] Zhaoqing Pan, Hao Zhang, Jianjun Lei, Yuming Fang, Xiao Shao, Nam Ling, and Sam Kwong. Dacnn: Blind image quality assessment via a distortion-aware convolutional neural network. *IEEE Transactions on Circuits and Systems for Video Technology*, 32(11):7518–7531, 2022.

- [35] Hamid R Sheikh, Muhammad F Sabir, and Alan C Bovik. A statistical evaluation of recent full reference image quality assessment algorithms. *IEEE Transactions on image processing*, 15(11):3440–3451, 2006.
- [36] Eric Cooper Larson and Damon Michael Chandler. Most apparent distortion: full-reference image quality assessment and the role of strategy. *Journal of electronic imaging*, 19(1):011006, 2010.
- [37] Nikolay Ponomarenko, Lina Jin, Oleg Jeremeiev, Vladimir Lukin, Karen Egiazarian, Jaakko Astola, Benoit Vozel, Kacem Chehdi, Marco Carli, Federica Battisti, et al. Image database tid2013: Peculiarities, results and perspectives. *Signal processing: Image communication*, 30:57–77, 2015.
- [38] Hanhe Lin, Vlad Hosu, and Dietmar Saupe. Kadid-10k: A large-scale artificially distorted iqa database. In *2019 Eleventh International Conference on Quality of Multimedia Experience (QoMEX)*, pages 1–3. IEEE, 2019.
- [39] Deepti Ghadiyaram and Alan C Bovik. Massive online crowdsourced study of subjective and objective picture quality. *IEEE Transactions on Image Processing*, 25(1):372–387, 2015.
- [40] Vlad Hosu, Hanhe Lin, Tamas Sziranyi, and Dietmar Saupe. Koniq-10k: An ecologically valid database for deep learning of blind image quality assessment. *IEEE Transactions on Image Processing*, 29:4041–4056, 2020.
- [41] Yuming Fang, Hanwei Zhu, Yan Zeng, Kede Ma, and Zhou Wang. Perceptual quality assessment of smartphone photography. In *Proceedings of the IEEE/CVF Conference on Computer Vision and Pattern Recognition*, pages 3677–3686, 2020.
- [42] Hugo Touvron, Matthieu Cord, and Hervé Jégou. Deit iii: Revenge of the vit. *arXiv preprint arXiv:2204.07118*, 2022.
- [43] Ramprasaath R Selvaraju, Michael Cogswell, Abhishek Das, Ramakrishna Vedantam, Devi Parikh, and Dhruv Batra. Grad-cam: Visual explanations from deep networks via gradient-based localization. In *Proceedings of the IEEE international conference on computer vision*, pages 618–626, 2017.

## A Qualitative Theoretical Justification

In our rigorous theoretical exploration, we have established that the loss function rooted in local manifold learning is superior to the traditional contrastive learning loss. By incorporating intra-class negative samples into our local manifold learning approach, we further diminish the mathematical expectation of the loss, as substantiated by Eq. 9.

$$\begin{aligned}
 & \because \mathbb{E}(|y - y_\varepsilon| - |y_\gamma - y_\delta|) \\
 &= \mathbb{E}(|y - (y + \varepsilon_\omega)| - |(y + \varepsilon_\gamma) - (y + \varepsilon_\delta)|) \\
 &= \mathbb{E}(|\varepsilon_\omega| + |\varepsilon_\gamma - \varepsilon_\delta|) \quad (\varepsilon_1 \leq \dots \leq \varepsilon_\omega \leq \dots \leq \varepsilon_n) \\
 &= \frac{1}{n} \sum_{\omega} |\varepsilon_\omega| - \frac{2}{n(n-1)} \sum_{\omega} (2\omega - n - 1)\varepsilon_\omega \\
 &= \begin{cases} \frac{1}{n}|\varepsilon_1| + \frac{2}{n}\varepsilon_1 \geq -\frac{1}{n}|\varepsilon_1|, & \omega = 1 \\ \frac{1}{n}|\varepsilon_n| - \frac{2}{n}\varepsilon_n \geq -\frac{1}{n}|\varepsilon_n|, & \omega = n \end{cases} \\
 & \therefore \mathbb{E}(|\varepsilon_\omega| + |\varepsilon_\gamma - \varepsilon_\delta|) \geq -|\varepsilon_\omega| \\
 & \therefore -|\varepsilon_\omega| \leq \mathbb{E}(|\varepsilon_\omega| + |\varepsilon_\gamma - \varepsilon_\delta|) \leq |\varepsilon_\omega| \\
 & \therefore ||y - y_\varepsilon| - |y_\gamma - y_\delta|| \leq ||y - y_\varepsilon||
 \end{aligned} \tag{9}$$

where  $y_\varepsilon$  represents the positive class, while  $y_\gamma$  and  $y_\delta$  denote inter-class negative classes. While our proofs predominantly operate at the score level, it's imperative to highlight that, owing to the functional mapping relationship between features and scores as depicted in Eq. 10, our proposed methodology retains its efficacy at the feature level. This also indicates that our method has the potential to be applied in more scenarios and maintain robustness.

$$\begin{aligned}
 & y = \mathcal{G}(f) \\
 & (y + \Delta y) \iff (f + \Delta f) \quad |\Delta y| \rightarrow 0, |\Delta f| \rightarrow 0 \\
 & \mathbb{E}(|y - y_\varepsilon| - |y_\gamma - y_\delta|) \iff \mathbb{E}(|f - f_\varepsilon| - |f_\gamma - f_\delta|),
 \end{aligned} \tag{10}$$

where  $f$  represents the feature,  $y$  denotes the quality score, and  $\mathcal{F}$  and  $\mathcal{G}$  signify the function mapping relationship.

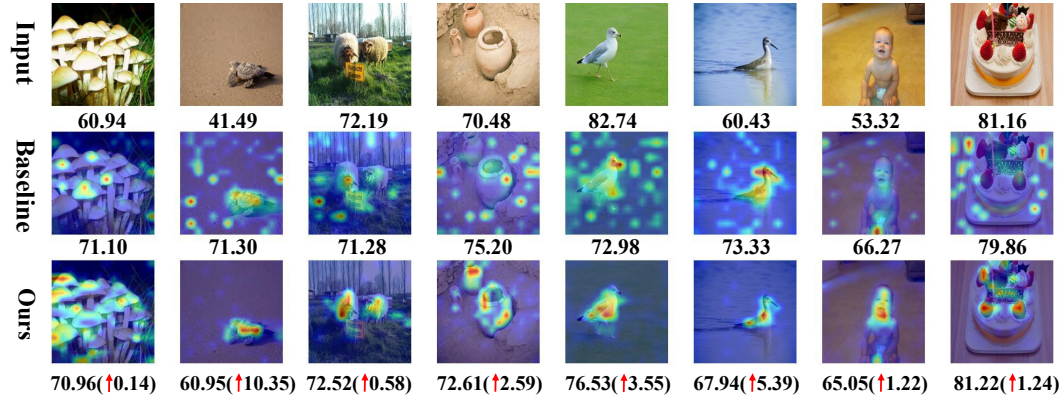


Figure 3: Activation maps of baseline [5] and LML-IQA using Grad-CAM. Rows 1-3 represent input images, CAMs generated by baseline, and generated by LML-IQA, respectively. The numbers below each row represent the Ground Truth, and the predicted scores of the baseline model and our model, respectively.

## B Visualization of Quality Attention Map

We employ GradCAM [43] to visualize feature attention maps, as depicted in Fig. 3. The visualization showcases our model's comprehensive and precise attention allocation to regions exhibiting significant visual distortion. In contrast, the baseline data tends to concentrate on non-target areas. This

observation underscores our model’s capacity to capture accurate semantic structures and attain more precise quality perception. Such a phenomenon arises from our deliberate emphasis on features from visual saliency regions throughout the training process. Furthermore, the prediction results for quality scores highlight our model’s superior image quality evaluation capability compared to the baseline, with the predicted scores closely aligning with the ground truth. In summary, these phenomena robustly underscore the efficacy of our proposed method.

## **C Limitations and Future Directions**

We primarily identify two avenues for improvement. Firstly, LML-IQA focuses on assessing the quality of real-world images, while temporarily overlooking the evaluation of images generated by generative models. Exploring how to integrate LML-IQA with AIGC to study a universal method for image quality assessment is a direction we aim to pursue in the future. Secondly, the visual saliency cropping can be further optimized, such as adaptively adjusting the cropping area size or increasing the number of crops to accommodate more diverse and complex distortion scenarios.